Physics in Medicine & Biology

IPEM Institute of Physics and Engineering in Medicine

**PAPER** • **OPEN ACCESS**

# On the microdosimetric characterisation of the radiation quality of a carbon-ion beam and the effect of the target volume thickness

To cite this article: Gabriele Parisi *et al* 2024 *Phys. Med. Biol.* **69** 245003

IOP Publishing Phys. Med. Biol. 69 (2024) 245003 https://doi.org/10.1088/1361-6560/ad965e

Physics in Medicine & Biology

IPEM Institute of Physics and Engineering in Medicine



OPEN ACCESS

RECEIVED
19 September 2024

REVISED
7 November 2024

ACCEPTED FOR PUBLICATION
22 November 2024

PUBLISHED
4 December 2024



PAPER

# On the microdosimetric characterisation of the radiation quality of a carbon-ion beam and the effect of the target volume thickness

**Gabriele Parisi**[1,2,3,*], **Giulio Magrin**[4], **Claudio Verona**[5], **Gianluca Verona-Rinati**[5], **Sandra Barna**[6], **Cynthia Meouchi**[7], **Francesco Romano**[8] and **Giuseppe Schettino**[2]

[1] Department of Physics, University of Surrey, Guildford, United Kingdom
[2] NPL—National Physical Laboratories, Teddington, United Kingdom
[3] Department of Physics, University of Pavia, Pavia, Italy
[4] MedAustron Ion Therapy Centre, Wiener Neustadt, Austria
[5] Department of Industrial Engineering, University of Roma 'Tor Vergata', Roma, Italy
[6] Department of Radiation Oncology, Medical University of Vienna, Vienna, Austria
[7] Department of Radiation Physics, Technische Universitat Wien, Vienna, Austria
[8] INFN—Istituto Nazionale di Fisica Nucleare, Sezione di Catania, Catania, Italy
[*] Author to whom any correspondence should be addressed.

**E-mail:** gabriele.parisi@unipv.it

**Keywords:** microdosimetry, diamond detectors, hadron therapy, carbon ions, radiation quality

## Abstract

*Objective.* Microdosimetry is gaining increasing interest in particle therapy. Thanks to the advancements in microdosimeter technologies and the increasing number of experimental studies carried out in hadron therapy frameworks, it is proving to be a reliable experimental technique for radiation quality characterisation, quality assurance, and radiobiology studies. However, considering the variety of detectors used for microdosimetry, it is important to ensure the consistency of microdosimetric results measured with different types of microdosimeters. *Approach.* This work presents a novel multi-thickness microdosimeter and a methodology to characterise the radiation quality of a clinical carbon-ion beam. The novel device is a diamond detector made of three sensitive volumes (SVs) of different thicknesses: 2, 6 and 12 $\mu$m. The SVs, which operate simultaneously, were accurately aligned and laterally positioned within 3 mm. This alignment allowed for a comparison of the results with a negligible impact of the SVs alignment and their lateral positioning, ensuring the homogeneity of the measured radiation quality. An experimental campaign was carried out at MedAustron using a carbon-ion beam of typical clinical energy (284.7 MeV u$^{-1}$). *Main results.* The measurement results allowed for a meticulous interpretation of its radiation quality, highlighting the effect of the SV thickness. The consistency of the microdosimetric spectra measured by detectors of different thicknesses is discussed by critically analysing the spectra and the differences observed. *Significance.* The methodology presented will be highly valuable for future experiments investigating the effects of the target volume size in radiobiology and could be easily adapted to the other particles employed in hadron therapy for clinical (i.e. protons) and for research purposes (e.g. helium, lithium and oxygen ions).

## 1. Introduction

Carbon-ion therapy is the second most widely used form of particle therapy after proton therapy, with an increasing number of clinical centres around the world (Particle Therapy Co-Operative Group—PTCOG www.ptcog.site). Compared with other radiation modalities such as X-rays or protons, carbon ions have several advantages supported by clinical evidence (Mohamad *et al* 2018). They are characterised by a narrower Bragg peak (BP) with a sharper fall-off (FO) potentially allowing for improved sparing of healthy tissues. They show an increased biological effectiveness in killing tumour cells, which increases their efficacy in treating radio-resistant tumours. In addition, some radiobiological properties of carbon ions might favour

positive reactions including enhanced immune response, decreased angiogenesis and lower risk of metastatic spread (Tinganelli and Durante 2020).

The radiation quality of a carbon-ion beam is particularly interesting and challenging to characterise. The significant amount of secondary fragments generated, coming from both target and projectile fragmentation, gives life to a very heterogeneous radiation field. Further, the extreme gradients found around the BP and along its FO require high position accuracy and excellent spatial resolution to be measured reliably.

Microdosimetry is an experimental radiation science measuring the stochastic interaction between radiation and matter in volumes with cell or sub-cellular sizes (Booz *et al* 1983, ICRU 2007). By characterising the stochastic energy deposition in cell-like volumes event-by-event, microdosimetry provides a very accurate description of the radiation quality of a specific radiation field (Lindborg and Waker 2017). Further, microdosimetric quantities can be directly linked to radiobiology, where increasing interest and effort have been made to develop dedicated microdosimetric-radiobiological models (Bellinzona *et al* 2021). The latest technological advancements of microdosimetry detectors have enabled an increasingly accurate and reliable application of microdosimetry to hadron therapy (Parisi *et al* 2022). In particular, solid state detectors are emerging as the ideal technology to characterise the radiation quality of carbon ions. Their micrometric size allows a spatial resolution of a few $\mu$m along the beam direction, otherwise not achieved by tissue-equivalent proportional counters. However, the lineal energy window over which a typical carbon-ion microdosimetric spectrum extends ranges from less than keV $\mu m^{-1}$ to thousands of keV $\mu m^{-1}$. This necessitates collecting charge pulses which amplitude spanning over many order of magnitude. It would be extremely challenging to develop one single detector with adequate sensitivity to collect events at a few keV $\mu m^{-1}$ with good resolution and also to collect events at thousands of keV $\mu m^{-1}$ without running into technological problems such as signal saturation or electric discharges. A reliable experimental method leading to an optimised characterisation of radiation quality is therefore needed. The combination of more than one microdosimetry technology, as suggested by Parisi *et al* (2022), might be an effective and versatile solution.

In this work, the combined use of microdosimeters of different thickness was investigated. The methodology presented relied on a novel diamond microdosimeter, specifically designed and developed for this purpose. Diamond microdosimeters are undergoing rapid progress and advancement, with the active development of innovative and increasingly reliable technologies (Verona *et al* 2015, 2018, 2022, 2024a, 2024b). The novel microdosimeter consisted of a single device made of three accurately aligned diamond detectors of 2, 6, and 12 $\mu$m thickness. A microdosimetric experiment was carried out at MedAustron (Wiener Neustadt, Austria) using a pristine 284.7 MeV $u^{-1}$ carbon-ion beam. Unlike other microdosimetry experiments carried out in similar conditions, the novel microdosimeter presented and employed in this work enabled simultaneous characterisation of the radiation quality for three different target-sizes. The results of the experiment were critically analysed and the impact of the target volume thickness to the microdosimetric quantities measured was discussed.

## 2. Material and methods

### 2.1. The microdosimeter

The experiments were carried out using a novel multi-thickness microdosimetric device specifically designed for the purpose of this work. Figures 1(a) and (b) show, respectively, its schematic representation and a microscope image of the three diamond detectors mounted on the electronic board. The device was made of three diamond microdosimeters based on the single-stage diamond detector technology developed by the University of Roma 'Tor Vergata', (Verona *et al* 2015, 2018). The device has an innovative configuration allowing simultaneous measurement with three sensitive volumes (SVs). The three diamond microdosimeters were manufactured by growing the SVs to different thicknesses, namely 2, 6 and 12 $\mu$m, on three substrates of equal thickness. In particular, for each detector, a boron-doped p-type layer of about 1 $\mu$m was grown by chemical vapour deposition (CVD) technique on the commercial high-pressure-high-temperature (HPHT) diamond substrate. The three HPHT diamond substrates were all $3 \times 3$ mm$^2$ in area and $0.30 \pm 0.06$ mm in thickness. The intrinsic diamond SV was subsequently grown to the desired thickness on the boron-doped diamond layer using the CVD growth technique. Finally, a very thin (about 50 nm) Chromium contact was patterned in a $100 \times 100$ $\mu$m$^2$ square shape on the intrinsic diamond layer using the photolithography technique. In order to create the multi-thickness microdosimeter, the three diamond samples (with cross-sectional area of $3 \times 3$ mm$^2$) were laser-cut by Almax easyLab to three identical pieces of $1 \times 3$ mm$^2$ area. The Chromium contacts were deposited to position one contact at the centre of each sample piece. One sample twin for each of the three detectors was then laid upon the same electronic board and they were fixed side by side to form a $3 \times 3$ mm$^2$ device made of three SVs of different thickness separated by a lateral distance of about 1 mm. The device was housed in a specifically designed metallic enclosure to screen

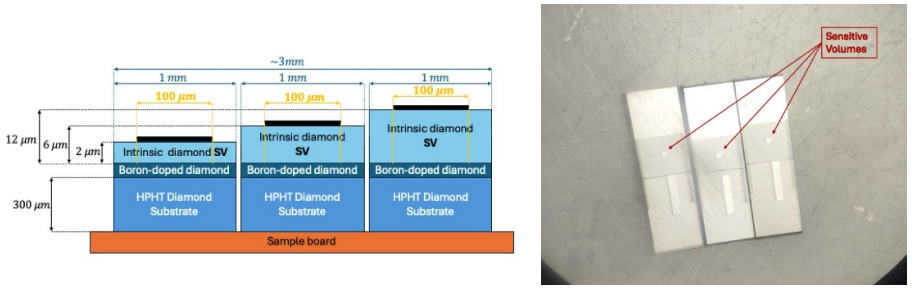


(a) (b)

**Figure 1.** (a) Schematic representation of the novel diamond multi-thickness microdosimetry device presented. (b) Picture of the three diamond microdosimeters before being laid and aligned on the same electronic board.

electromagnetic noise and disturbances. The enclosure was equipped with three BNC connectors to connect the detectors to the electronics and with a 1 cm window hole centred on the three diamond detectors. The whole device was eventually embedded into epoxy resin to make it waterproof, thus usable in conventional water phantoms. The uncertainty of the three SVs regarding alignment along the irradiation axis (i.e. their placement at the same depth with respect to the particle beam) was estimated by the manufacturer to be lower than 0.1 mm, considering their fabrication process. The relatively small sensitive area of each detector, namely $100 \times 100\ \mu m^2$, allowed excellent performance in terms of pile-up at clinical fluence rates. The device was operated without noticeable pile-up distortion up to fluence rate of the order of $1 \times 10^8\ cm^{-2}\ s^{-1}$. It is important to underline that a comparable diamond-based microdosimeter demonstrated stable performance up to a fluence rate of $1.7 \times 10^9\ cm^{-2}\ s^{-1}$, as reported by Verona *et al* (2015). The charge collection efficiency (CCE) exhibited an exponential decrease under high cumulative doses, with a characteristic decay constant of approximately 4.8 MGy for carbon ions. This indicated a strong radiation hardness of thin-layer diamond microdosimeters and demonstrated their suitability for daily quality control applications. Radiation damage also depends on the detector's thickness: a thicker microdosimeter would experience increased damage due to the longer drift distance of charge carriers in the active region.

The performance of these detectors was preliminary tested by means of ion beam induced charge experiments at the Surrey Ion Beam Centre (Guildford, UK), employing micro-beams of low energy helium and carbon ions. The detectors showed an excellent definition of their SV with a good homogeneity of charge collection throughout the sensitive area and approximately 100% CCE.

### 2.2. The experiments at MedAustron

The experiments were carried out at the MedAustron hadron-therapy centre in Wiener Neustadt (Austria), using a 284.7 MeV $u^{-1}$ carbon-ion beam. A solid-water phantom composed of RW3 slabs of calibrated thickness was used to simulate the desired water-depth. The microdosimetric system, positioned behind the solid-water slabs, was aligned with the beam axis using the facility's positioning lasers. The front surface of the first RW3 slab was placed at the irradiation isocentre. The detector position was fixed at a distance of 5 mm from the rear surface of the thickest set of RW3 slabs used: the required RW3 thickness required to simulate the deepest depth planned (165 mm) was set, and the microdosimeter was placed 5 mm behind it. The experimental set-up is shown in figure 2. The thickness of epoxy resin in front of the detector SVs, estimated to be 1 mm, was also considered when calculating the thickness of RW3 required to obtain the planned water depth for the measurements. The water-equivalent thickness (WET) of RW3 slabs had been previously measured by MedAustron researchers, while the WET of the epoxy layer was calculated using stopping power tables.

Each of the three SVs was connected to an analogous conventional amplification chain made of an Amptek 'CoolFET' A250CF charge-sensitive pre-amplifier and an ORTEC 671 shaping amplifier. The amplified signal was read by an ORTEC 927 multi-channel analyser, communicating to a PC using ORTEC's software MAESTRO. A shaping time of 2 $\mu$s was used for all detectors. The amplification gain was set independently for each SV to obtain the highest sampling resolution (highest amplification gain), allowing detection over the whole linear energy range expected. The built-in pile-up rejection system of the ORTEC amplifier was used.

An external voltage was applied to the SVs to ensure their correct operation. The operational bias voltage suggested by the manufacturer to obtain a fully depleted sensitive volume was applied to the three detectors. Hence, 2.5, 18, and 36 V were supplied to the 2, 6, and 12 $\mu$m detectors, respectively. The voltage applied to the 2 $\mu$m SV was lower than its nominal operating voltage (6 V). This was necessary since electronic

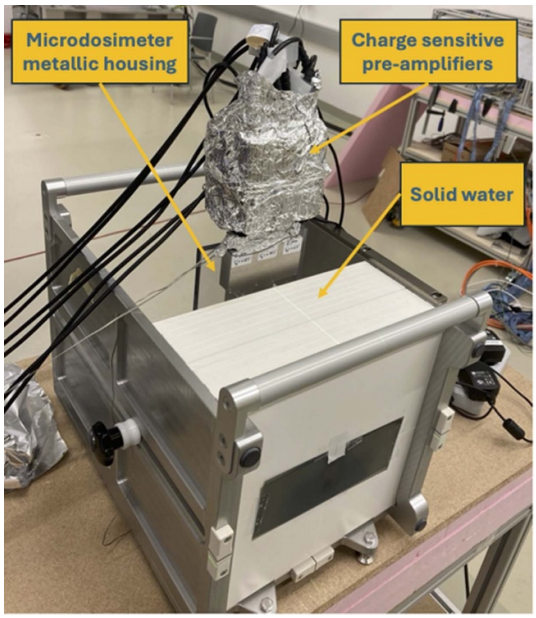


**Figure 2.** Experimental set-up at MedAustron. The detector is placed behind the RW3 slabs.

discharges were observed when supplying the nominal voltage. The origin of this problem was not clear, even though it might be related to a possible damage to the metallic electrodes or to the micro-wires connecting them to the front-end electronics. These might have occurred during the device transportation or during setup operations. Nonetheless, this issue had only a marginal impact on the results and discussions presented by this work. The operational consequence of using a lower bias voltage, indeed, is a non-perfect depletion of the sensitive volume, translating to a possible reduction of sensitive volume thickness, which should not be higher than 0.5 $\mu$m. Hence, this issue would not affect the following discussion since the 2 $\mu$m thick SV is already the thinnest detector.

### 2.3. Data analysis

*2.3.1. Microdosimetry formalism*

The fundamental quantity of microdosimetry is the lineal energy $y$. Following its definition in the ICRU (Booz *et al* 1983, Braby 2023): the lineal energy is the quotient of $\varepsilon_s$ by $\bar{l}$, where $\varepsilon_s$ is the energy imparted to matter into a given volume by a single-event energy deposition, and $\bar{l}$ is the mean chord length in that volume. A single-event energy deposition is the energy deposited by correlated charged particles: the primary particle and all its secondaries. In some cases, as initial proposed by Bolst *et al* (2017) and further thoroughly discussed in the latest ICRU report on Microdosimetry (Braby 2023), the mean chord length might not be representative of the path traveled by the particle depositing energy into the volume. Thus, the use of the mean path length $l_\mathrm{p}$ is suggested. The experimental scenario of this work, involving a highly directional beam crossing a non-isotropic volume, is one of these cases. For a straight ion beam traversing a slab-shaped volume, the mean path length is equal to the volume thickness. Hence, a $l_\mathrm{p} = t_\mathrm{det}$ where $t_\mathrm{det}$ is the detector thickness, was considered the most appropriate choice. The lineal energy is conventionally represented through the so-called lineal energy dose distribution $d(y)$, which is defined as:

$$\mathrm{d}(y) = \frac{y}{\bar{y}_F} f(y) \tag{1}$$

where $f(y)$ is the lineal energy probability density function and $\bar{y}_F$ its expectation value, called frequency-mean lineal energy. Hence $\bar{y}_F = \int_0^\infty y f(y) \mathrm{d}y$. The lineal energy dose distribution is usually reported in a semi-logarithmic plot, as this highlights different features of the spectrum.

The second momentum of the frequency distribution, which corresponds by definition to the expectation value of $\mathrm{d}(y)$, is called dose-mean lineal energy $\bar{y}_D$ and it is one of the most important microdosimetric quantities. $\bar{y}_D$ is defined as:

$$\bar{y}_D = \int_0^\infty y \mathrm{d}(y)\, \mathrm{d}y = \frac{1}{\bar{y}_F} \int_0^\infty y^2 f(y)\, \mathrm{d}y. \tag{2}$$

Experimental measurements are affected by a low lineal energy threshold due to background noise, disturbances or technological limitations. The lowest lineal energy value measurable is therefore different than 0, thus the definition of $\bar{y}_F$ and $\bar{y}_D$ cannot be strictly met by a measurement. Following the concepts presented in Lindborg and Waker (2017), the *truncated* $\bar{y}_F$ and *truncated* $\bar{y}_D$ are introduced. The two quantities, denoted respectively as $\bar{y}_F^t$ and $\bar{y}_D^t$, are defined as:

$$\bar{y}_F{}^t = \int_{y_{\text{low}}}^{\infty} y f(y)\,\mathrm{d}y \tag{3}$$

$$\bar{y}_D^t = \int_{y_{\text{low}}}^{\infty} y \mathrm{d}\,(y)\,\mathrm{d}y = \frac{1}{\bar{y}_F{}^t}\int_{y_{\text{low}}}^{\infty} y^2 f(y)\,\mathrm{d}y \tag{4}$$

where $y_{\text{low}}$ is the low lineal energy threshold, or cut-off, of the specific measurement.

*2.3.2. Experimental data processing*

The experimental data collected were analysed to obtain the microdosimetric quantities of interest. The microdosimeter measures current pulses proportional to the energy deposited by a single-event. These are integrated in voltage pulses by the pre-amplifier and further amplified by the shaping amplifier. The results obtained need to be calibrated to retrieve the original deposited energy information. Firstly, the data collected were linearised to account for the amplification chain response. The linearisation was performed following the double-linearisation method proposed by Meouchi *et al* (2022), which minimise the uncertainty contribution of the linearisation. The double-linearisation method relies on the function:

$$a_{\text{lin}} = \begin{cases} a_{\text{ch}} m_A + q & \text{if } a_{\text{ch}} \leqslant a_{\text{T}} \\ a_{\text{ch}} m_B + q + (m_A - m_B)\, a_{\text{T}} & \text{if } a_{\text{ch}} > a_{\text{T}} \end{cases} \tag{5}$$

where $a_{\text{lin}}$ is the linearised signal amplitude, $a_{\text{ch}}$ is the signal amplitude in acquisition-channels units and $m_A$, $m_B$ and $q$ are the three linearisation coefficients. $a_{\text{T}}$ is a free parameter which is chosen to minimise the sum of the squares of the residuals when fitting the linearisation data obtained by employing a pulse generator. The linearisation coefficients were obtained by fitting equation (5) to a set of linearisation data measured for the purpose using the TGF4242 pulse generator by AIM-TTI Instruments. The final calibration in lineal energy was then obtained according to the carbon-edge method. The particle-edge method (Crossman and Watt 1994, Conte *et al* 2013) is the conventional calibration technique used in microdosimetry. Since it uses a very well-defined feature of the spectrum (the particle-edge: the highest energy that the particle could possibly deposit in the detector SV), the calibration can be done during each experiment to ensure a calibration coefficient reliably accounting for the specific experimental conditions, thus minimising the contribution of systematic errors. The carbon-edge value was calculated from the stopping power values of carbon ions in carbon provided by ICRU-73 (ICRU 2005), according to the method described by Chiriotti *et al* (2015), Meouchi *et al* (2022). The carbon-edge values 2565 keV $\mu$m$^{-1}$, 2310 keV $\mu$m$^{-1}$ and 2034 keV $\mu$m$^{-1}$ were obtained for the 2 $\mu$m, 6 $\mu$m and 12 $\mu$m thick diamond detectors, respectively.

The calibrated data obtained are eventually organised in the form of a histogram with logarithmic lineal energy bins. The frequency and dose distributions, and their expectation values, are calculated following the microdosimetry formalism.

The microdosimetric results presented in this manuscript were reported without any density normalisation and without any shape or material conversion (i.e. diamond with density 3.51 g cm$^{-3}$ and slab geometry).

*2.3.3. Uncertainty calculation*

The uncertainties were calculated according to the law of propagation of uncertainty, following the guide to the expression of uncertainty in measurement (GUM) uncertainty framework by the International Bureau of Weights and Measures (BIPM)'s GUM (JCGM 100:2008 2008). The sources of uncertainty were propagated to the final uncertainty by considering a first-order approximation of the measurement function Taylor series. In uncertainty theory, the measurement function is defined as the mathematical formula, step-by-step calculation procedure, or any other prescription which allows to obtain the final results from the input quantities. Thus, by indicating the measurement function as $M_f$, the final result $Y$ of the measurement is obtained as $Y = M_f(X_i)$, where $X_i$ are the different input quantities. The final uncertainty $u_C(Y)$ was calculated as:

$$\begin{cases} u_C(Y) = \sqrt{\sum_i (c_i^2 u^2(X_i))} \\ c_i = \frac{\delta M_f(X_i)}{\delta X_i} \end{cases} \tag{6}$$

where $u(X_i)$ is the standard uncertainty of the input quantity $X_i$.

For what concerns the microdosimetry uncertainty, the only source of type A uncertainty was the counting statistics. The radiation counting process is well-known to follow Poisson statistics. In each lineal energy bin, the number of counts $N$ of lineal energy events was therefore associated with a standard uncertainty of $\sqrt{N}$ according to the Poisson distribution. Besides, the lineal energy values uncertainty was the combination of the uncertainty of the linearisation and calibration coefficients, and of the sensitivity of the digital sampling. The calibration and linearisation coefficients were obtained by fitting dedicated data: a set of signal pulses of several known amplitudes sent to the pre-amplifier by a pulse generator, processed by the whole electronic chain and measured for the linearisation coefficients; and a microdosimetric spectrum collected at a measurement point where the carbon-edge was neat and well populated (for instance, along the FO). Their standard uncertainty was calculated considering the uncertainty associated with the fit-coefficients and an estimated uncertainty of the stopping power values used to estimate the carbon-edge value. It is generally accepted that in a typical energy range of a clinical carbon beam the uncertainty of tabulated stopping power values is about 5%, as also suggested by Ziegler *et al* (2010). It must be remarked that the values of the linearisation coefficients are known to vary with different linearisation-fit methods. Even though only the uncertainty related to the mathematical fit procedure was considered, it has been shown that a systematic error related to the choice of the linearisation-fit method exists (Meouchi *et al* 2022). This particularly affects low lineal-energy channels. The systematic error is related to the amplification electronics, so it equally affected the results measured by the 3 detectors. Thus, while it did not influence the comparison shown and the discussions presented, it did impact the absolute values measured at low lineal energy (i.e. at the entrance). These are therefore to be taken with an uncertainty higher than what reported on this work to account for the systematic error. As the sensitivity of the digital sampling was the unit channel and its uncertainty thus characterised by a rectangular distribution, its standard uncertainty was $\frac{1}{2\sqrt{3}}$ channels.

Besides microdosimetry uncertainties, the other important uncertainty to address is the one of the water equivalent depth at which the measurement was carried out. This was estimated as the combination of the uncertainty of:

1. the water-equivalent thickness of the epoxy layer in front of the detector's SV, which was estimated as the combination of the dead-layer thickness measured by a x-ray radiography with 250 $\mu$m sensitivity, and of the water-equivalent conversion uncertainty;
2. the water-equivalent thickness of the RW3 slabs used as moderator, which had been experimentally measured by other researchers at MedAustron with an uncertainty of 1% of the real RW3 thickness.

Since the water-equivalent conversion coefficient was calculated as the ratio of two tabulated stopping power values with 5% uncertainty (Ziegler *et al* 2010), its uncertainty was the 7.07%. It can be demonstrated, indeed, that the relative uncertainty of an output quantity obtained by the ratio of two input quantities is equal to the square-root of the sum of the squares of the two input uncertainty. Hence, if $k_{we}$ is the water-equivalent conversion coefficient, $\sigma(k_{we})$ its uncertainty, $SP_w$ and $SP_{rw3}$ the two stopping power values, and $\sigma(SP_w)$ and $\sigma(SP_{rw3})$ their uncertainties: $\frac{\sigma(k_{we})}{k_{we}} = \sqrt{\left(\frac{\sigma(SP_w)}{SP_w}\right)^2 + \left(\frac{\sigma(SP_{rw3})}{SP_{rw3}}\right)^2} = \sqrt{2 \cdot 0.05^2} = 0.0707$.

Table 1 summarises the sources of uncertainty considered for both microdosimetric quantities and the measurement of the water equivalent depth. Those sources of uncertainty were propagated to the final uncertainty following equation (6), in accordance with the GUM uncertainty framework.

## 3. Results: experimental microdosimetry

The microdosimetric measurements were carried out employing a different thickness of RW3 slabs, reproducing different water-equivalent depths. The microdosimetric measurements were carried out at different depths along the depth-dose profile as indicated in figure 3. The results which were critically discussed focused on the four different water-equivalent depths highlighted with a golden circle in figure 3. These were representative of the four main regions of a carbon-ion Bragg curve: the entrance, the BP, the peak FO, and the distal tail (DT). The corresponding lineal energy distributions measured by the three SVs are shown in figure 4. Figure 5 reports instead the microdosimetric spectra measured by the 6 $\mu$m SV at all the depths investigated.

The excellent alignment of the three detectors was reflected in the good agreement observed between the peak position measured by the three SVs at all depths. The peak position corresponds to the most probable lineal energy value. As shown by figure 4, the radiation quality measured by SVs of different thickness varies around a relatively well preserved most probable lineal energy value. The microdosimetric spectra features

**Table 1.** Sources of uncertainty considered for the two experiments carried out at MedAustron, their distribution and their standard uncertainty. The standard uncertainty corresponds to the standard deviation of the distribution of the source of uncertainty (input quantity). For a rectangular distribution, the standard deviation is defined as $\frac{1}{\sqrt{3}}\frac{b-a}{2}$, where $b-a$ is the distribution width.

| Input quantity | Distribution | Standard uncertainty |
|---|---|---|
| Microdosimetry | | |
| Counting statistics | Poisson | $\sqrt{N_i}$ |
| Double-Linearisation coefficient $m_A$ | Gaussian | <1% [a] |
| Double-Linearisation coefficient $m_B$ | Gaussian | <1% [a] |
| Double-Linearisation coefficient $q$ | Gaussian | 30%–60% [a] |
| Calibration coefficient $k$ | Gaussian | 5%–9% * |
| Bin width of original histogram | Rectangular | 0.29 channels |
| Water-equivalent thickness | | |
| Epoxy layer thickness | Rectangular | 0.07 mm |
| Epoxy water-equivalent conversion factor | Gaussian | 0.08 mm |
| Water-equivalent thickness of RW3 slabs $t_{RW3}$ | Gaussian | $0.01 t_{RW3}$ |

$N_i$ is the number of counts in the $i$th bin.

[a] precise value according to system. The uncertainty of the linearisation and calibration coefficients were not reported precisely because they were different for each combination of detector, acquisition system, and amplification gain used.

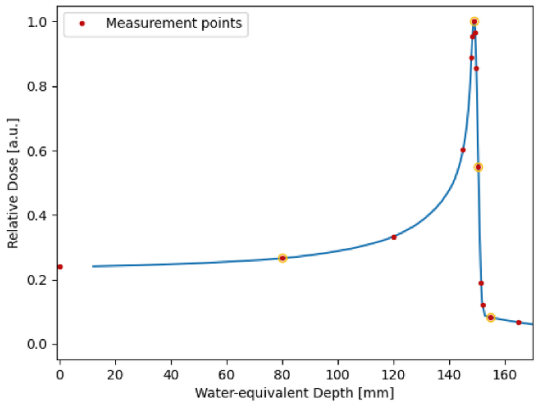


**Figure 3.** Depth-dose profile of the 284.7 MeV u$^{-1}$ carbon-ion beam employed for the experiment. The curve was measured by the MedAustron's calibrated ionisation chamber dosimeter. The golden circled points show the four measurement points showed in the comparison between the three microdosimeters with different thickness.

were also preserved and are therefore to be univocally attributed to the specific radiation quality, regardless of the SV thickness. This highlights the suitability and reliability of microdosimetry to characterise the radiation quality. Some experimental issues limited the accuracy of the measurements. The low lineal energy threshold was generally too high to measure the whole contribution from lighter secondary fragments of higher energies (i.e. depositing very low lineal energy). The DT region, where the radiation quality is exclusively made of secondary fragments, is the most affected region. A more detailed discussion of the impact of the low lineal energy threshold in microdosimetry could be found in Bianchi *et al* (2021). Since the low lineal energy threshold is an intrinsic limit of experimental microdosimetry, different techniques have been proposed to extrapolate the missing part of the microdosimetric spectrum down to 0 keV $\mu$m$^{-1}$. To be a clinically relevant correction, the extrapolation method must have a strong physical basis. A possible meticulous solution was proposed by Verona *et al* (2024a), who developed a device to simultaneously perform the microdosimetry and the dosimetry. The part of the spectrum below the threshold could be reconstructed by ensuring it represents the fraction of dose associated with those events, which could be estimated as the difference between the measured dose and the dose calculated from the microdosimetric measurement (which intrinsically considers only events above the detection threshold). However, it is out of the scope of this work to discuss extrapolation techniques. No extrapolation was carried out on the data presented in order to discuss the purely experimental observations. The threshold issue was particularly problematic for the 2 $\mu$m detector, making it blind along most of the entrance region. Such misbehaviour of the 2 $\mu$m detector is believed to be the result of some undesired electronic disturbance from the surrounding

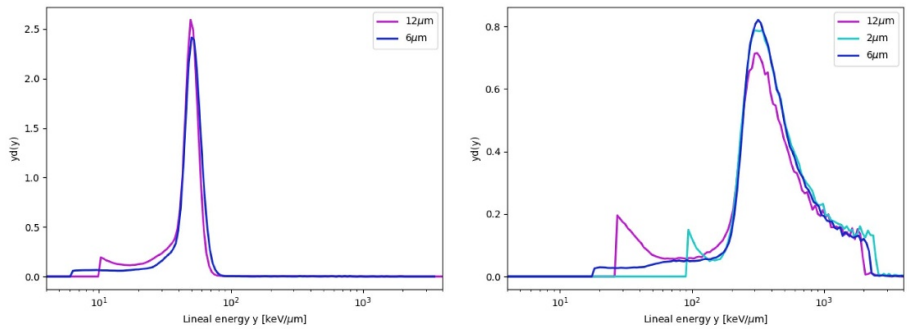


(a) Water-equivalent depth of 80 mm: entrance.




(b) Water-equivalent depth of 149 mm: Bragg peak.

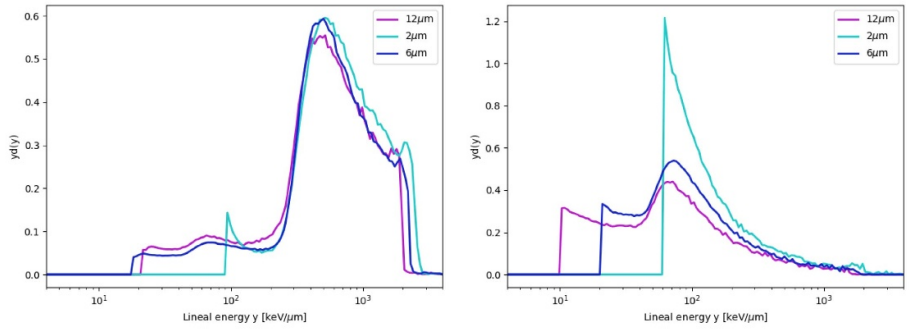


(c) Water-equivalent depth of 150.5 mm: Fall-off.




(d) Water-equivalent depth of 155 mm: Distal tail.

**Figure 4.** Microdosimetric spectra of a 284.7 MeV u$^{-1}$ carbon-ion beam, measured by the diamond microdosimeters at different water-equivalent depths.

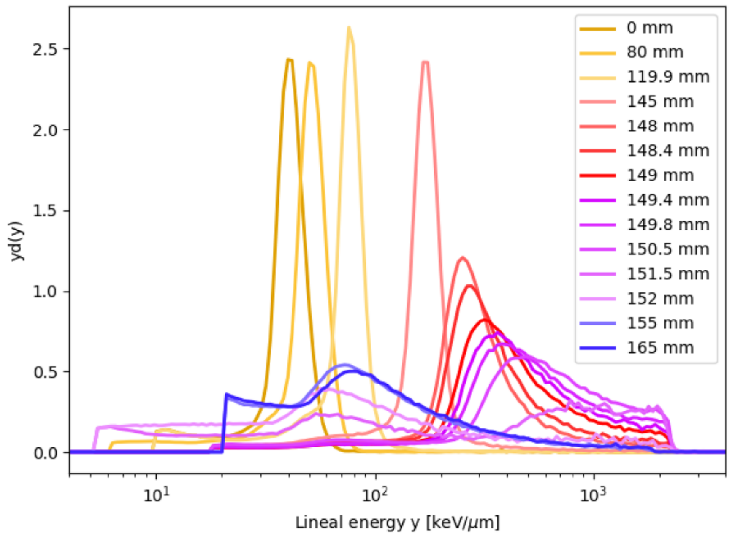


**Figure 5.** Microdosimetric spectra of a 284.7 MeV u$^{-1}$ carbon-ion beam, measured by the 6 $\mu$m microdosimeter at different water-equivalent depths along the whole depth-dose profile.

environment affecting either the detector or its electronic chain and adding to the background electronic noise. This might also be driven by the same issue preventing the detector from operating at its nominal applied voltage without discharging.

The $\bar{y}_F^t$ and $\bar{y}_D^t$ values measured are reported in table 2. A common lineal energy cut-off was set equal to the highest between the experimental cut-off value of the three microdosimeters. This allowed for a meaningful comparison between the three different thicknesses. The application of the common cut-off was carefully performed to ensure that the main parts of the spectra were correctly taken into account. In the DT, since the highest lineal energy threshold, which was the one of the 2 $\mu$m detector, cut half of the main spectrum peak out, the common cut-off was set equal to the threshold value of the 6 $\mu$m detector and the $\bar{y}_F^t$

**Table 2.** $\bar{y}_F^t$ and $\bar{y}_D^t$ values of a 284.7 MeV u$^{-1}$ carbon-ion beam, measured at different water-equivalent depths. The values reported were calculated considering a common low lineal energy cut-off between the three detectors of 25 keV $\mu$m$^{-1}$ for the measurements at 80 and 155 mm and of 80 keV $\mu$m$^{-1}$ for the measurements at 149 and 150.5 mm.

| Region | WE depth (mm) | 2 $\mu$m thick SV (keV $\mu$m$^{-1}$) | 6 $\mu$m thick SV (keV $\mu$m$^{-1}$) | 12 $\mu$m thick SV (keV $\mu$m$^{-1}$) |
|---|---|---|---|---|
| | | $\bar{y}_F$ | | |
| Entrance | $80.0 \pm 0.8$ | — | $49 \pm 3$ | $47 \pm 3$ |
| Bragg peak | $149.0 \pm 1.5$ | $369 \pm 19$ | $367 \pm 19$ | $347 \pm 18$ |
| Fall-off | $150.5 \pm 1.5$ | $509 \pm 26$ | $474 \pm 24$ | $436 \pm 22$ |
| Distal tail | $155.0 \pm 1.6$ | — | $73 \pm 4$ | $73 \pm 4$ |
| | | $\bar{y}_D$ | | |
| Entrance | $80.0 \pm 0.8$ | — | $53 \pm 3$ | $50 \pm 3$ |
| Bragg peak | $149.0 \pm 1.5$ | $591 \pm 30$ | $546 \pm 28$ | $531 \pm 27$ |
| Fall-off | $150.5 \pm 1.5$ | $850 \pm 43$ | $763 \pm 39$ | $712 \pm 36$ |
| Distal tail | $155.0 \pm 1.6$ | — | $157 \pm 8$ | $155 \pm 8$ |

and $\bar{y}_D^t$ values measured by the 2 $\mu$m detector were not considered. The higher common cut-off resulted in a general over-estimation of the real $\bar{y}_F$ and $\bar{y}_D$ by the measured $\bar{y}_F^t$ and $\bar{y}_D^t$ values.

Finally, figure 5 compellingly shows the evolution of the radiation quality, i.e. the microdosimetric spectra, with increasing depth in water. The rate of change increases, reaching the BP and continuing along the FO, which can be clearly appreciated.

## 4. Discussion: interpretation of the radiation quality measured by microdosimeters of different thickness

The results obtained enabled an interesting discussion on the optimisation of the radiation quality characterisation of a carbon beam using detectors of different thicknesses.

The exceptional sensitivity of microdosimetry to radiation-quality changes, combined with the high rate of change of radiation quality with depth for a carbon-ion beam, makes the relative position between the SVs a critical parameter to manage carefully. A previous experiment carried out with different devices revealed that an alignment uncertainty of about 0.5 mm was not sufficient for this purpose. A relative positioning uncertainty lower than 0.1 mm was required to obtain a meaningful comparison between detectors. This device was able to achieve such precision in detector alignment.

The experimental results obtained were analysed and carefully interpreted to discuss the impact of the SV thickness on the radiation quality as described by microdosimetry.

A general behaviour of the $\bar{y}_D^t$ difference between thinner and thicker detectors could be observed. $\bar{y}_D^t$ was systematically higher for thinner detectors along the whole depth-dose profile (DDP). In the DT, however, the impact of the low lineal energy threshold might affect the comparison. Since a relevant part of the microdosimetric spectrum was missing, the actual differences in $\bar{y}_D^t$ are expected to be higher than those observed. A deeper analysis focused on each of the four main regions of a carbon-ion beam's DDP follows. As indicated by Lindborg and Waker (2017), it is useful to consider the lineal energy as affected by several contributions to the overall energy deposition variance, which determine the microdosimetric spectrum shape. These contributions could be summarised as the variances related to several factors: the particle LET, the energy-loss straggling, the secondary electrons ($\delta$-rays) escape, the path length distribution, and the experimental factors. By indicating the variance of the factor $i$ as $V_i$, the contributions mentioned will be referred to as, respectively: $V_L$, $V_S$, $V_\delta$, $V_{\mathrm{pl}}$ and $V_{\mathrm{exp}}$. For a slab-shaped detector exposed to a unidirectional radiation field, $V_{\mathrm{pl}}$ is mainly determined by the scattering the particle undergoes crossing the detector, by those particles stopping inside the detector, and by the non-perfect unidirectionality of the radiation field (scattering outside the detector). $V_{\mathrm{exp}}$ encompasses experimental factors that may influence the measured value of lineal energy. These factors include charge recombination, charge discharges, electromagnetic noise, pile-up, and saturation. Without correction methods, these factors act as systematic effects tied to the experimental conditions. They do not represent a specific source of uncertainty but instead alter the shape of the measured microdosimetric spectrum, reducing measurement precision. The contribution of $V_\delta$ in a slab detector with a relatively high aspect ratio (100:6) is expected to be less important than other variances. In particular, when describing the differences between the spectra measured by an SV with thicknesses differing by a few $\mu$m and equal cross-sectional area of $1 \times 10^4$ $\mu$m$^2$, the contribution of $V_\delta$ to the microdosimetric spectra is negligible.

### 4.1. Entrance

In the entrance region, the primary carbon ions have relatively low LET values, thus their range is much longer than the detectors' thickness. It is therefore reasonable to assume that all primaries cross the detectors' SV. Since the beam scattering for carbon ions in this region is minimal, the contribution from $V_{\mathrm{pl}}$ is expected to be almost negligible. The spectrum is mainly delineated by the combination of $V_L$, $V_S$, and $V_{\mathrm{exp}}$. The entrance region is characterised by very mild LET gradients. This makes it reasonable to confidently assume negligible variations in the primary ions' LET as they cross the detectors' thickness. Hence, $V_L$ is expected to give a similar contribution to the microdosimetric spectra measured by detectors of different thickness. $V_S$ is therefore the main factor affecting the impact of the SV's thickness on the microdosimetric spectrum. Relying on the work of Kellerer and Chmelevsky (1975), the variance due to the energy-loss straggling varies with the particle path length which, in this case, is the detector thickness. In particular: $V_S \propto \frac{1}{l_p}$. A broader spectrum is therefore expected from thinner detectors. As shown in figure 4(a), the expected behaviour was indeed observed. By fitting the frequency distribution $f(y)$ with a Gaussian function, the full-width-half-maximum was 16.0 keV $\mu$m$^{-1}$ and 14.0 keV $\mu$m$^{-1}$ for, respectively, the 6 $\mu$m and 12 $\mu$m microdosimeters. However, while the effect was clear on the right-hand side of the lineal energy peak, the left-hand side of the two measured spectra was fairly similar. This is not surprising and can be explained by considering $V_{\mathrm{exp}}$. $V_{\mathrm{exp}}$ contributes to broadening the experimental spectra with respect to an ideal case, especially at lower lineal-energy values where the electronic noise has a higher impact. The effect of the different contributions of $V_S$ between the detectors was therefore weakened by $V_{\mathrm{exp}}$, which is not expected to have a strong dependence on the detector thickness. The radiation-quality differences observed resulted in an increasing $\bar{y}_D^t$ value for decreasing SV thickness. This is explained by considering that, since to calculate $\bar{y}_D$ the dose-distribution is weighted on the lineal energy its-self, the right-hand side of the lineal energy peak at higher lineal energy gives a stronger contribution to $\bar{y}_D$. Hence, while the left-hand side was smoothed by $V_{\mathrm{exp}}$, the thinner detectors reached further on the higher lineal-energy side because of the different contribution of $V_S$, leading to an increase of $\bar{y}_D$. Even though the $\bar{y}_D^t$ variation fell within the measurement uncertainty, the $\bar{y}_D^t$ measured by the 6 $\mu$m detector was more than 5% higher than the $\bar{y}_D^t$ measured by the 12 $\mu$m detector, supporting the interpretation of the spectra given. The results obtained were consistent, for the thickness range investigated, with those found by Bolst *et al* (2020) following a computational study of the impact of the detector thickness for silicon microdosimeters.

### 4.2. Bragg Peak

Moving towards the BP, the kinetic energy of primary ions decreases. The evolution of the microdosimetric spectrum can be neatly observed in figure 5. A ledge at higher lineal energy appears towards the BP. Its contribution increases with depth and it populates a lineal energy region reaching the ion-edge. The ion-edge corresponds to the maximum energy that can be deposited by a specific charged particle into a volume of a certain thickness. This condition is usually reached when the ion's kinetic energy is approximately the value corresponding to a range equal to the detector thickness. Hence, the presence of a noticeable ion-edge indicates the presence of primaries stopping within the detector. The presence of the ion-edge introduces an important difference between the microdosimetric spectra measured by SVs of different thicknesses. The ion-edge position is found at significantly higher lineal-energy values for thinner SVs. The carbon-edge, for example, is found at 2565 keV $\mu$m$^{-1}$ for a 2 $\mu$m thick diamond detector, at 2310 keV $\mu$m$^{-1}$ for a 6 $\mu$m detector, and 2034 keV $\mu$m$^{-1}$ for a 12 $\mu$m detector. The carbon-edge values reported were calculated using a continuous slowing down approximation, using stopping power values from ICRU-73 (ICRU 2005). The carbon-edge position extends the microdosimetric spectrum of thinner detectors towards higher lineal energy, increasing the value of $\bar{y}_D^t$ with respect of a thicker detector. Observing figures 4(b) and (c), the increase in $\bar{y}_D^t$ for thinner detectors becomes intuitive since, while the edge position noticeably shifts towards higher lineal energy, the height of the edge region does not change significantly between detector thicknesses.

Towards the BP, the increase of LET gradients is appreciable. However, the LET increase in a 10 $\mu$m diamond detector was estimated from stopping power tables to be generally $< 1\%$ and to get to a maximum of 2% only at the BP. Hence, in this case, $V_L$ had only a marginal contribution to the differences of lineal energy distribution related to the different thickness of the detectors.

According to Kellerer and Chmelevsky (1975), $V_S$ could be expressed as:

$$V_S = \frac{2m_e E}{\bar{\epsilon} M \ln \frac{4m_e E}{MI}} \propto \frac{E}{\bar{\epsilon} \ln E} \tag{7}$$

where $m_e$ is the electron mass, $M$ is the ion mass, $I$ is the mean ionisation potential for the target material, $\bar{\epsilon}$ is the mean imparted energy, and $E$ is the ion's kinetic energy. Towards the BP, the kinetic energy of the primaries decreases and the mean imparted energy increases, causing $V_S$ to decrease. $V_S$ becomes comparable to $V_{\mathrm{pl}}$, lowering its impact to the spectral differences observed using different SV's thicknesses.

As observed in figure 4(b), the major contribution to the variations due to the detector thickness around the BP was the edge-region, in accordance with the discussion above.

### 4.3. Fall-Off

Climbed over the BP, the scenario along the FO is very similar but all features are enhanced. This could be well appreciated in figure 5.

As the primaries' kinetic energy decreases, $V_S$ becomes negligible. The LET gradients ramp up to an extent that could appreciably impact the variations of the microdosimetric spectrum due to different detector thicknesses. From stopping power tables, the LET increase when crossing a 10 $\mu$m thick diamond detector at the bottom of the FO was estimated to be higher than the 15% of the impinging LET. The effect of such high LET variations is challenging to predict as it strictly depends on the detector configuration. A perfect alignment is assumed to simplify the discussion. Considering the microdosimeter structure, as represented in figure 1(a), the SVs alignment was created on their back surface. At very high LET, the LET distribution at the entrance of the three SVs could be different. The same distribution at the epoxy surface is moderated by a certain epoxy thickness $e_0$, common for all three detectors, before entering the thicker SV. However, the LET distribution entering a thinner detector is further moderated by an epoxy thickness corresponding to $\Delta t = t_\mathrm{T} - t_\mathrm{t}$, where $t_\mathrm{T}$ is the thickness of the thicker SV, and $t_\mathrm{t}$ the thickness of the thinner. The energy deposited in the thicker detector would see a contribution from the first $\Delta t$ and a contribution from the remaining $t_\mathrm{t}$. Assuming a comparable energy deposition in diamond and epoxy, the energy deposited into the thinner detector would have only the contribution from its thickness $t_\mathrm{t}$, but the particle still loses energy in the $\Delta t$ travelled in epoxy. Since in the FO the LET has very high gradients, the additional contribution from $\Delta t$ seen by the thicker detector is expected to weight its microdosimetric distribution towards lower lineal energy values. Even though only a minor effect was expected, a difference in position of the spectra peaks and a decrease of the $\bar{y}_D^t$ measured by thicker microdosimeters can be observed in figure 4(c) and table 2, respectively.

Moving along the FO, as shown in figure 5, the contribution from the edge-region increases significantly. The impact of the differences in the edge position between different SV's thicknesses is therefore enhanced, increasing the $\bar{y}_D^t$ measured by thinner detectors.

The fraction of primaries stopping into the SV increases as well. A stopper travels a shorter path than a crosser, intrinsically increasing the path length variance $V_\mathrm{pl}$. The lineal energy measured from a stopper is inaccurate as the length used in its definition, which aims to represent the path travelled by the ion into the target volume, is not representative of the real path length of the stopper. The energy deposited by a stopper along its real track length $l_\mathrm{r} < t$ is weighted on a longer path. Hence, the lineal energy of the same event results in being lower when measured by a thicker SV into which the particle stops than in the case of a SV which is thin enough to be crossed. The fraction of stoppers depends on the kinetic energy of the ion entering the SV and on the SV thickness. In particular, it is higher, thus producing greater inaccuracy, at deeper positions along the FO and in thicker detectors.

Down the FO an increasing number of primaries stop before reaching the detector, thus the contribution from secondary fragments increases. In the case of carbon ions, nuclear fragments are mainly lighter ions with higher energies (thus longer ranges and lower LET). Unfortunately, the experimental results obtained were not suitable to accurately study the effect of their contribution as the low lineal energy threshold cut out a relevant part of their spectrum. However, in the spectra measured by the 6 $\mu$m and 12 $\mu$m detectors in figure 4(c), a contribution from fragments was clearly visible. Considering the importance of an accurate characterisation of secondary fragments and their effects, a microdosimetry investigation focused on secondary fragments is envisaged for the future.

### 4.4. Distal tail

In the distal tail region the radiation quality is made of secondary fragments only, since all primary ions have stopped. The transition from FO to DT is particularly well represented in figure 5, where a drastic reduction of primaries fraction could be clearly observed in the span of less than 2 mm. This region of transition between FO and DT, occurring in this case between 150.5 mm and 152 mm depth, resulted the region with the strongest microdosimetric spectra variation rate per depth. This makes the FO-DT transition region particularly critical in the treatment planning and in the evaluation of the biological effectiveness of the treatment.

The scenario in the DT changes drastically from the FO. The secondary fragments of a carbon-ion beam include both the projectile's fragments, which are necessary to be lighter than the projectile, and the target's fragments. Since the target was water (and similarly in a real treatment with tissues), whose heaviest atomic component is oxygen, most of the target's fragments were also lighter than carbon. Fragments are produced with a kinetic energy of the same order as the primary's to fulfil the energy conservation. Hence, as the

charge of the fragments was lower than the charge of the primary, the field of secondaries was characterised by much lower LET than the primary's. The microdosimetric spectrum changes significantly, spreading towards lower lineal energy values. The low lineal energy threshold became a relevant issue as it could be appreciated in figure 4(d). The comparable side of the spectra, however, matched well with a slight shift of the peak towards higher lineal energies for thinner detectors. A clear ion-edge was also observed by all detectors, respecting the edge position differences between different detector thicknesses previously discussed. The ion-edge appearing in the DT is related to the secondary fragments species. By fitting the edge structure, its position well agreed with the lineal energy expected for the boron-edge, showing a relevant contribution from boron fragments at this depth. The presence of the boron-edge in the DT of a therapeutic carbon-ion beam was first reported by Meouchi *et al* (2022, 2024).

The $\bar{y}_D^t$ value measured by thinner detectors was found to be higher. The effects observed in this region could be thought of as a sort of ensemble of what was observed in the other regions. The part of the spectrum related to the lighter fragments (i.e. protons, and helium) captures the characteristics of the entrance region, with a leading contribution from $V_S$ to the lineal energy differences between different SV's thicknesses. At the same time, heavier ions such as boron, are characterised by higher lineal energy depositions generating a part of the spectrum more similar to the primary BP and its FO. Differences of the ion-edge position were therefore observed as well. In addition, since fragments are not strictly produced in the same direction of the primaries which generated them, $V_{\mathrm{pl}}$ is expected to deviate from the uni-directionality of the primary beam. This is expected to consequently create an inaccuracy in the lineal energy measured since the mean path length considered is less representative of the actual track length of the particle depositing energy. Finally, since the low lineal energy threshold hindered a non-negligible part of the spectra, the differences between the $\bar{y}_F^t$ and $\bar{y}_D^t$ values measured with a lower lineal energy threshold by SVs with different thickness are expected to be higher than what observed for their values reported in table 2.

Dose gradients in the DT are notoriously very mild, as they are at the entrance. As it could be observed by looking at the spectra measured at 155 and at 165 mm by the 6 $\mu$m detector and shown in figure 5 the variations of microdosimetric spectrum with depth in the DT are very mild as well.

## 5. Conclusions

The work presents a successful experimental method to characterise the radiation quality of an ion beam in terms of microdosimetry, considering SVs of different thickness. The method relies on a novel diamond microdosimeter: a single device made of three detectors placed onto the same sample-board, thus intrinsically aligned. The detectors were 2, 6 and 12 $\mu$m thick. The methodology was employed to carry out a microdosimetry experiment at MedAustron hadron-therapy centre using a pristine carbon-ion beam of 284.7 MeV u$^{-1}$. The results of the experiment are presented. Thanks to the data collected, a critical analysis of the radiation quality of a carbon-ion beam was conducted, focusing on the impact of the target volume thickness. The radiation quality was described by means of microdosimetry, analysing the four main regions of a carbon-ions depth-dose profile: the entrance, the BP, the FO, and the distal tail (DT).

Following the discussion, a suggestion on how to optimise the radiation-quality measurement of a carbon-ion beam using microdosimeters of different thickness is given:

- in the entrance region, a fairly-thick detector (4–6 $\mu$m) should be used to measure a whole and clear spectrum above the detection threshold, minimising the noise distortion.
- in the BP and along its FO, a thinner detector (0.5–3 $\mu$m) is suggested to maximise the spatial resolution, while minimising the lineal energy inaccuracy caused by primaries stopping inside the SV.
- in the DT, a thicker detector (6–12 $\mu$m) is needed to measure the whole lineal energy range of the secondaries, down to very low lineal energy values.

However, care must be taken when microdosimetry is used to specifically characterise nuclear fragments. A thinner detector is suggested for this purpose as, besides reducing the fraction of heavier fragments stopping into the SV, it would reduce the number of nuclear interactions occurring into the detector SV, which contaminates the secondary field measured.

It is important to highlight that the shape of the microdosimetric spectra and their features are well preserved for different SV's thicknesses up to at least 12 $\mu$m. This ensures consistency in the characterisation of the radiation quality. Hence, any SV thickness could be reliably used for quality assurance or radiation-quality comparison purposes (such as between different hadron-therapy centres, different delivery strategy, etc), as long as detectors with the same thickness are employed.

The situation changes when microdosimetry is applied to radiobiology, where the specific parts of the spectrum are directly linked to the biological effects. Since appreciable differences in the microdosimetric

spectrum and mean values were observed for different SV thicknesses, the most representative SV size to describe biological effects cannot exclusively rely on the detector performance. This is crucial, especially in the entrance and FO regions, where the higher differences were observed. However, the most representative site size to link to radiobiological effects is still an open question attracting the interest of many researchers. The experimental methodology presented could give an invaluable contribution to this research quest when used in combination with radiobiological experiments

Finally, the results of the experiment also allowed some observations on the novel multi-thickness microdosimeter. The low lineal energy threshold was a relevant issue impacting the accuracy of the experimental method investigated. This is the weak point of solid-state detectors in general. A significant effort should be put into improving the performance of the multi-thickness microdosimeter and its electronics to lower the threshold as much as possible. Its impact could indeed compromise the microdosimetric quantities measured, especially for thinner detectors in the DT and in the entrance region. For a proton beam measurement, the impact of the low lineal energy threshold would be even higher (as protons deposit lower lineal energy than carbon ions). Provided that good statistics are measured, the highest contribution to the final uncertainty comes from the calibration factor. An alternative calibration method could be investigated to improve this uncertainty. If the calibration method does not rely on stopping power tables, the highest contribution to the calibration uncertainty would be eliminated. For instance, the detector could be calibrated in deposited energy by irradiating it with a particle field of known energy (such as a mono-energetic ion beam) and ensuring the particle stops inside the SV, thus releasing all of its kinetic energy. The use of multiple calibration points along the whole lineal energy range measured would also mitigate the linearisation uncertainty and systematic errors.

In conclusion, the results of this work allowed a meticulous microdosimetric interpretation of the radiation quality of a typical carbon-ion beam used in hadron therapy, as measured by SVs of different thicknesses. The results of the study provided a reliable methodology to measure the radiation quality of a carbon-ion beam for quality assurance purposes and to study the effects of the target volume size in radiobiology. This will be fundamental for the development of more robust and consistent radiobiological models.

## Data availability statement

All data that support the findings of this study are included within the article (and any supplementary files).

## Acknowledgments

This work was funded by EPSRC industrial CASE award.

The experiments carried out for this work were possible thanks to a collaboration between National Physical Laboratories (NPL) and MedAustron.

## ORCID iDs

Gabriele Parisi https://orcid.org/0000-0001-5777-1269
Giulio Magrin https://orcid.org/0000-0002-0920-0477
Claudio Verona https://orcid.org/0000-0001-6401-3765

## References

Bellinzona V E, Cordoni F, Missiaggia M, Tommasino F, Scifoni E, La Tessa C and Attili A 2021 Linking microdosimetric measurements to biological effectiveness in ion beam therapy: a review of theoretical aspects of MKM and other models *Front. Phys.* **8** 578492

Bianchi A, Selva A, Colautti P, Parisi A, Vanhavere F, Reniers B and Conte V 2021 The effect of different lower detection thresholds in microdosimetric spectra and their mean values *Radiat. Meas.* **146** 106626

Bolst D, Guatelli S, Tran L T, Chartier L, Lerch M L, Matsufuji N and Rosenfeld A B 2017 Correction factors to convert microdosimetry measurements in silicon to tissue in $^{12}$C ion therapy *Phys. Med. Biol.* **62** 2055–69

Bolst D, Guatelli S, Tran L T and Rosenfeld A B 2020 The impact of sensitive volume thickness for silicon on insulator microdosimeters in hadron therapy *Phys. Med. Biol.* **65** 035004

Booz J, Braby L, Coyne J, Kliauga P, Lindborg L, Menzel H G and Parmentier N 1983 ICRU report 36: microdosimetry *J. Int. Comm. Radiat. Units Meas.* **os19** NP

Braby L A *et al* 2023 ICRU report 98, stochastic nature of radiation interactions: microdosimetry *J. ICRU* **23** 1–168

Chiriotti S, Moro D, Conte V, Colautti P, Grosswendt B, Sterpin E and Vynckier S 2015 Influence of the physical data to calibrate tepcs *Radiat. Prot. Dosim.* **166** 238–41

Conte V, Moro D, Grosswendt B and Colautti P 2013 Lineal energy calibration of mini tissue-equivalent gas-proportional counters (TEPC) *AIP Conf. Proc.* **1530** 171–8

Crossman J S P and Watt D E 1994 Inherent calibration of microdosemeters for dose distribution in lineal energy *Radiat. Prot. Dosim.* **55** 295–8

ICRU 2005 *ICRU Report 73, Stopping of Ions Heavier than Helium* (International Commission on Radiation Units and Measurements)
ICRU 2007 *ICRU Report 78: Prescribing, Recording, and Reporting Proton-Beam Therapy* (International Commission on Radiation Units and Measurements)
JCGM 100:2008 2008 *Evaluation of Measurement Data—Guide to the Expression of Uncertainty in Measurement* (Joint Committee for Guides in Metrology) (available at: www.bipm.org/documents/20126/2071204/JCGM_100_2008_E.pdf)
Kellerer A M and Chmelevsky D 1975 Criteria for the applicability of let *Radiat. Res.* **63** 226–34
Lindborg L and Waker A 2017 *Microdosimetry* (CRC Press) (https://doi.org/10.1201/9781315373737)
Meouchi C, Barna S, Puchalska M, Tran L T, Rosenfeld A, Verona C, Verona-Rinati G, Palmans H and Magrin G 2022 On the measurement uncertainty of microdosimetric quantities using diamond and silicon microdosimeters in carbon-ion beams *Med. Phys.* **49** 6699–715
Meouchi C, Barna S, Rosenfeld A, Tran L T, Palmans H and Magrin G 2024 Microdosimetry of a clinical carbon-ion pencil beam at medaustron—part 1: experimental characterization
Mohamad O, Yamada S and Durante M 2018 Clinical indications for carbon ion radiotherapy *Clin. Oncol.* **30** 317–29
Parisi G, Romano F and Schettino G 2022 Microdosimetry for hadron therapy: a state of the art of detection technology *Front. Phys.* **10** 1035956
Tinganelli W and Durante M 2020 Carbon ion radiobiology *Cancers* **12** 3022
Verona C, Barna S, Georg D, Hamad Y, Magrin G, Marinelli M, Meouchi C and Verona-Rinati G 2024a Diamond based integrated detection system for dosimetric and microdosimetric characterization of radiotherapy ion beams *Med. Phys.* **51** 533–44
Verona C, Magrin G, Solevi P, Bandorf M, Marinelli M, Stock M and Verona-Rinati G 2018 Toward the use of single crystal diamond based detector for ion-beam therapy microdosimetry *Radiat. Meas.* **110** 25–31
Verona C, Magrin G, Solevi P, Grilj V, Jaksic M, Mayer R, Marinelli M and Verona-Rinati G 2015 Spectroscopic properties and radiation damage investigation of a diamond based schottky diode for ion-beam therapy microdosimetry *J. Appl. Phys.* **118** 184503
Verona C, Parisi G, Cesaroni S, Crnjac A, Jaksic M, Marinelli M, Palomba S, Romano F, Schettino G and Verona-Rinati G 2022 Characterisation of a monolithic $\Delta E$-$E$ diamond telescope detector using low energy ion microbeams *Radiat. Meas.* **159** 106875
Verona C, Verona-Rinati G, Schettino G and Parisi G 2024b Development and fabrication of microdosimeter arrays based on single-crystal diamond Schottky diodes *Phys. Status Solidi* a **221** 2300987
Ziegler J F, Ziegler M D and Biersack J P 2010 SRIM—the stopping and range of ions in matter (2010) *Nucl. Instrum. Methods Phys. Res.* B **268** 1818–23